Traveling waves in the Northern Hemisphere of Mars

R. John Wilson,[1] Don Banfield,[2] Barney J. Conrath,[2] and Michael D. Smith[3]

[1]   Analysis of temperature retrievals from Mars Global Surveyor Thermal Emission Spectrometer data has revealed the presence of regular, eastward propagating waves in the Northern Hemisphere. A large amplitude, zonal wave 1 with a long (∼20 sol) period is particularly prominent during early winter ($L_s = 220-270°$). After $L_s = 270°$, a weaker and more rapidly propagating (6.5 sol period) zonal wave 1 is dominant. These waves have a deep vertical structure (>40 km) correlated with the axis of the winter hemisphere westerly jet. Simulations with a Mars general circulation model suggest that the fast wave is associated with baroclinic instability due to the strong meridional temperature gradient at the surface and is consistent with surface pressure oscillations seen in Viking Lander data. By contrast, the slow wave has the appearance of a large-amplitude Rossby wave that is coupled with an inertially unstable region in the subtropics.   INDEX TERMS: 5409 Planetology: Solid Surface Planets: Atmospheres—structure and dynamics; 5445 Planetology: Solid Surface Planets: Meteorology (3346); 6225 Planetology: Solar System Objects: Mars; 3384 Meteorology and Atmospheric Dynamics: Waves and tides

1.   Introduction

[2]   Planetary-scale traveling waves in the martian atmosphere have been inferred from observations by the two Viking Landers. Surface pressure data indicated waves with periods of 2 to 10 sols (martian days) and the associated wind and temperature perturbations are consistent with eastward-propagating, planetary-scale, quasi-geostrophic eddies with zonal wavenumbers of 1–4 [*Barnes*, 1980, 1981]. These waves were present during the northern hemisphere (NH) fall, winter, and spring seasons when strong midlatitude westerly zonal flow is expected. Temporal power spectra derived from Viking Lander 2 surface pressure observations (48°N) indicate a series of well-defined peaks, in contrast to the relatively flat spectra associated with terrestrial wave activity [*Collins et al.*, 1996]. Mars global circulation model (MGCM) simulations have yielded transient baroclinic eddies with periods similar to the Viking observations [*Barnes et al.*, 1993; *Collins et al.*, 1996]. MGCM simulations further suggest that the structure of transient zonal wavenumbers 1 and 2 is particularly deep (∼40 km) and should be amenable to observation from orbiting spacecraft [*Barnes et al.*, 1993].

[1]NOAA/Geophysical Fluid Dynamics Laboratory, Princeton, New Jersey, USA.
[2]Department of Astronomy, Cornell University, Ithaca, New York, USA.
[3]NASA Goddard Space Flight Center, Greenbelt, Maryland, USA.

[3]   The analysis of Mariner 9 infrared sounder data [*Conrath*, 1981] suggested the presence of a planetary wave structure embedded in the polar vortex, however, the limited observations were unable to distinguish between traveling waves and a stationary zonal wave 2. Mars Global Surveyor (MGS) Thermal Emission Spectrometer (TES) is currently providing retrievals of atmospheric temperature profiles with unprecedented latitude and longitude coverage suitable for characterizing the seasonal evolution of stationary and traveling planetary waves [*Banfield et al.*, 2002]. TES data from the first year of mapping has enabled the first unambiguous identification of traveling waves in the martian atmosphere [*Banfield et al.*, 2000, 2001; *Barnes*, 2001]. An analysis and interpretation of some of these results is presented here. We find that transient atmospheric temperature variability during the NH winter season is dominated by an eastward-propagating zonal wave 1 that appears to undergo a rapid transition from a slowly propagating state to a more rapidly propagating state. We also investigate the character of the traveling waves in a MGCM simulation that bear a reasonable correspondence with the observed waves. This simulation provides a means of relating the observations to simulated temperature and dynamical structures, yielding insight into the eddy circulations and their energetics.

2.   MGS TES observations

[4]   The sun-synchronous orbit of the MGS spacecraft provides 12 daily observations each at 2 am and 2 pm local solar time, spaced ∼30° in longitude. Temperature profiles have been derived from TES spectra using the retrieval algorithm described in *Conrath et al.* [2000]. These retrievals extend from the surface to 0.1 mb (∼40 km), with a vertical resolution ranging from ∼10 km near the surface to ∼15 km at higher altitudes. Figure 1a shows the time evolution of zonally averaged midlevel (∼0.5 mb) temperature (T_{15}) during the NH fall and winter season of the first year of the MGS mapping mission. A typical temperature cross section is shown in Figure 1b. The pronounced meridional gradient in the NH defines the boundary of the polar vortex, a strong westerly jet (Figure 1c) in gradient wind balance with the temperature field. In spite of a regional scale dust storm at $L_s = 225-235°$ and the changing season, the latitude-height structure of NH zonal mean temperature (and zonal wind) does not vary appreciably throughout this period.

[5]   Figure 2a shows the evolution of the longitude structure of T_{15} at 62.5°N, revealing the presence of both stationary and traveling waves. The wave 2 component is dominated by a stationary wave [*Banfield et al.*, 2002] which maintains a steady phase throughout the fall to spring season while stationary zonal wave 1 is most evident after $L_s = 260°$. We have isolated transient waves by removing
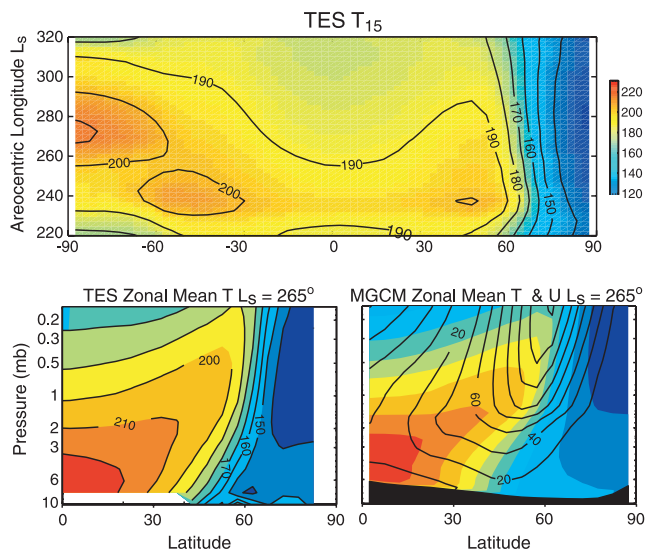
Figure 1. (a) Zonally-averaged midlevel temperature, T_{15} as a function of latitude and season. T_{15} is a depth-weighted temperature centered at ∼0.5 mb (∼25 km) [*Wilson*, 2000]. The time of year is represented by areocentric longitude (L_s), which is defined as zero at the vernal equinox, 90° at NH summer solstice etc. (b) Representative latitude-height section of zonal mean temperature ($L_s = 265°$) from TES retrievals. (c) Comparable zonal mean temperature (color) and zonal mean zonal winds (contours) from a MGCM simulation. The contour interval is 20 ms^{-1}.

running means from each longitude bin. The results are not sensitive to the averaging interval (20 sols) employed. For example, Figure 2b shows the evolution of the transient wave 1 component of T_{15}. This field has a standing wave response immediately following the dust storm event at $L_s = 225°$ that evolves into a slowly eastward propagating wave that dominates the $L_s = 240–265°$ interval. A more rapidly eastward propagating, but weaker amplitude, wave emerges after solstice. Similar coherent wave behavior is seen at other pressure levels.

[6] We have employed a correlation algorithm to characterize the traveling waves in the TES temperature retrievals. Specifically, we correlate synthetic traveling waves (varying zonal wavenumber and phase speed) with the transients at each pressure level to identify the amplitude and phase of the waves that best match the data. This analysis confirms that the $L_s = 240–270°$ and $L_s = 275–320°$ intervals are each dominated by an eastward propagating zonal wave 1 with a well-defined phase speed and vertical structure. The period of the large amplitude slow wave is ∼20 sols while the period of the low amplitude fast wave is ∼6.5 sols, corresponding to phase speeds (at 60°N) of 6 and 18.5 ms^{-1}, respectively. The amplitude and phase structures are shown in Figures 3a and 3b. In both cases, the maximum in eddy amplitude is correlated with the axis of the circumpolar jet and there are only modest relative phase variations in latitude and height. The analysis indicates the presence of the fast wave 1 during the interval when the slow wave is prominent, but only in the lowest few kilometers. We have also detected the presence of weak (∼2 K) and relatively shallow eastward propagating zonal waves 2 and 3. The

phase speed of wave 2 is comparable to that of the fast wave 1, consistent with coherent eddy propagation.

3. Mars GCM Simulations

[7] In this section we present results from a MGCM simulation with a slowly decaying dust distribution that resulted in a seasonal variation of zonal mean temperature in good agreement with the observations shown in Figure 1. The MGCM has been described in *Wilson and Hamilton* [1996] and comparisons with MGS data are described in *Wilson* [2000] and *Hinson and Wilson* [2002]. This simulation yielded a traveling wave response in the NH dominated by a large amplitude, eastward propagating zonal wave 1 with a 10 sol period during $L_s = 230–270$, and a weaker 6.7 sol period wave 1, prominent during $L_s = 280–330$. The latitude-height structures of these slow and fast waves are shown in Figures 3c and 3d, respectively. The amplitudes tend to maximize along the poleward flank of the circumpolar jet. The comparison with the observations (Figures 3a and 3b) indicates that the amplitudes and eddy structures above 3 mb are quite similar for both wave states. The fast wave is also present during $L_s = 230–270°$ in the
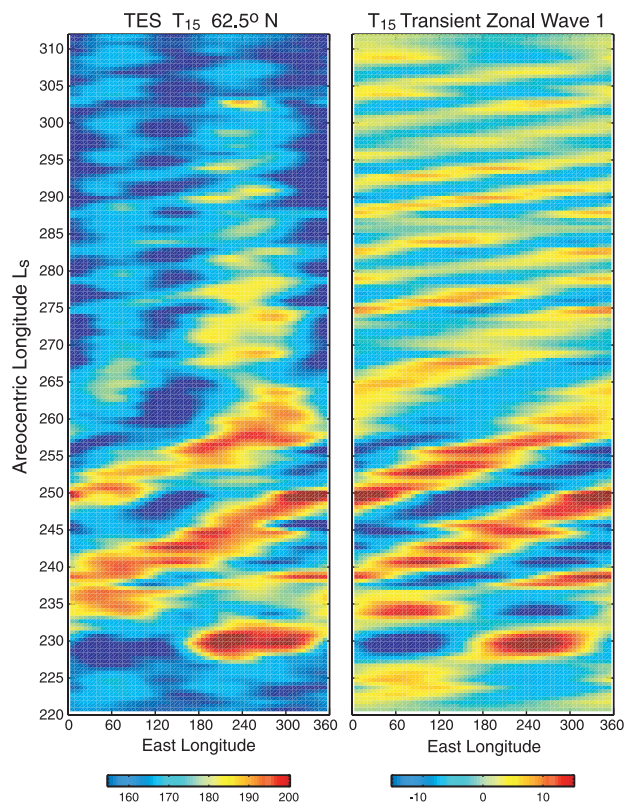

Figure 2. (a) Longitude vs. L_s variation of 2 am T_{15} at 62.5°N. Day and night side temperatures have been processed separately and the same pattern is evident in both data sets. Longitude variations have been fitted to Fourier components with waves 0 to 4. (b) The corresponding transient zonal wave 1 component, obtained by removing a 20-sol running mean from zonal wave 1. A slowly eastward propagating wave (20 sol period) is prominent for $L_s = 240–265°$ while a more rapidly propagating (6.5 sol period) wave emerges after solstice.
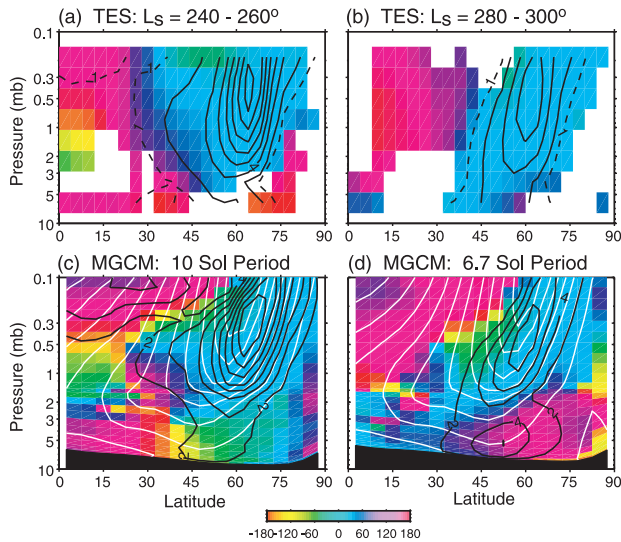
Figure 3. Vertical structure of the (a) long period (~20 sol) and (b) short period (6.5 sol) eastward propagating zonal wave 1 components of TES temperature. Contours represent amplitude at 2 K intervals (the 1 K contour is dashed) and color indicates relative phase in degrees longitude. The slow (10 sol period) and fast (6.7 sol period) wave structures from the MGCM simulation are shown in panels c and d, respectively. Zonal wind is shown with white contours in 20 ms^{-1} intervals, as in Figure 1c.

simulation, but with weaker amplitude (4 K vs. 8 K) above the 3 mb level than during L_s = 280–330°. Although the simulated slow wave has half the period of the observed slow wave, it is distinct from the fast wave and shares similar structural features with the observed slow wave. The observed and simulated slow wave structures (Figures 3a and 3c) have a high altitude temperature response extending to the equator. A preliminary analysis of TES limb temperature profiles yields a more prominent tropical eddy amplitude (~3 K) at 0.1 mb than shown in Figure 3a, presumably due to improved vertical resolution at these pressures. Note that the simulated tropical temperature structure in Figure 3c indicates a phase variation with height that might be smoothed by observations with limited vertical resolution.

[8] The simulated fast wave (Figure 3d) is distinguished by an enhanced near-surface response not evident in either of the slow wave structures (Figures 3a and 3c) or in the observed fast wave structure. The structure in Figure 3d is consistent with the simulated eddy temperature variance field shown in Figure 9c in *Barnes et al.* [1993] which is also dominated by an eastward propagating zonal wave 1 with a ~7 sol period. Notably, the surface pressure signal of the simulated fast wave dominates that of the slow wave despite having a weaker maximum in temperature amplitude. The mass-weighted contribution of the near-surface temperature response accounts for the dominance of the 6.7 sol wave in the surface pressure signal. By contrast, the simulations suggest that the eddy temperature structures deduced from TES data lack sufficient mass-weighted amplitude to account for surface pressure oscillations of the amplitude observed at the Viking Lander sites. It is likely that the vertical smoothing inherent in the TES

retrievals accounts for the absence of an enhanced near-surface temperature response in Figure 3b.

[9] The simulation indicates that the amplitudes of the eastward propagating components of zonal waves 2 and 3 are weaker than for wave 1 (consistent with the TES analysis) and are largely confined to below 3 mb. Other simulations with the MGCM have typically yielded eastward propagating surface pressure anomalies with periods of ~7 sols, 3–4 sols and ~2 sols, dominated by zonal waves 1, 2, and 3, respectively. These periods are comparable to those observed by the Viking landers [*Barnes*, 1980, 1981] and are consistent with other MGCM results [*Barnes et al.*, 1993; *Collins et al.*, 1996; *Hollingsworth et al.*, 1997]. Changes in the period of surface pressure variations are found to be associated with transitions in the dominant zonal wavenumber characterizing the eddy structure, as was noted by *Collins et al.* [1996]. Notably, long period waves are not evident in the Viking surface data. Plots of simulated near-surface eddy fields (not shown) indicate coherent propagation of the eddy structure as a well-defined low pressure center with prominent warm and cold fronts. The simulated surface pressure variations at 48°N are ~0.2 mb, in rough agreement with observed eddy pressure amplitudes at Viking Lander 2 [*Barnes*, 1981].

4. Discussion

[10] In this section we further discuss differences in the character of the simulated slow and fast waves. The simulated fast waves (zonal waves 1, 2 and 3) tilt westward with height in the lower atmosphere and have near-surface temperature maxima at the level where the wave phase speed (~20 ms^{-1}) matches the zonal-mean zonal velocity (Figure 3c). These features are characteristic of baroclinic waves associated with strong near-surface wind shear [*Barnes*, 1984]. The meridional and vertical fluxes of heat and momentum associated with the fast waves are similar to those described by *Barnes et al.* [1993]. By contrast, slow wave 1 has a deep, large amplitude structure with a relatively weak near-surface temperature response. This structure has
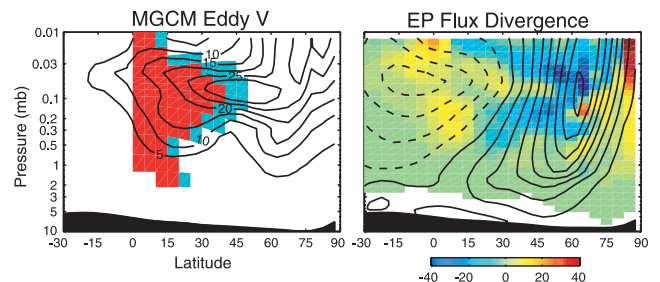

Figure 4. (a) Amplitude structure of meridional wind for the simulated slow wave. The contour interval is 5 ms^{-1}. Shading indicates the region where the poleward gradient of zonal-mean angular momentum on isentropic surfaces is positive, satisfying the condition for inertial instability. Red (blue) indicates the region where the zonal mean (zonal mean + wave 1) gradient is positive. (b) Divergence of Eliassen-Palm flux for the simulated slow wave. This field is dominated by the divergence of meridional momentum flux, u'v'. Shaded units are ms^{-1}sol^{-1}. Contours indicate zonal-mean zonal wind field in 20 ms^{-1} increments.

the character of a Rossby wave centered in the midlatitude wave guide established by the circumpolar jet. MGCM and linear model studies have indicated that a slowly propagating zonal wave 1 Rossby mode may be resonantly enhanced in the presence of a suitable zonal mean flow [*Hollingsworth and Barnes*, 1996; *Barnes et al.*, 1996]. Thus the identification of a slowly propagating wave in the TES data appears to be a confirmation of these predictions.

[11] Figure 4a shows that the meridional wind field of the simulated slow wave extends to the equator and is located in a region where the isentropic gradient of angular momentum increases toward the pole. This reversal of the "normal" gradient fulfills the necessary condition for inertial instability and presents a broad latitude range that offers weak resistance to meridional motion [*Andrews et al.*, 1987]. The slow wave momentum structure is distinct from the much smaller scale inertial circulations found by *Barnes et al.* [1993] associated with fast baroclinic waves. At any given longitude, the eddy meridional circulation represents a temporal modulation of the Hadley circulation. Simulations with an axisymmetric version of the MGCM reveal an oscillating meridional circulation with a latitude-height structure similar to that in the MGCM simulation. The axisymmetric model circulation is clearly a finite amplitude manifestation of inertial instability, with an oscillation period dependent on the intensity of the thermal forcing. A period of ~10 sols is obtained for dust loading comparable to that in the 3D simulation. Figure 4b shows the divergence of Eliassen-Palm flux due to the simulated slow wave. This field is dominated by the divergence of eddy meridional momentum flux ($-u'v'$), and strong barotropic energy conversion from the zonal mean flow is implied [*Andrews et al.*, 1987]. Such conversion is consistent with inertially-unstable circulations. We also find evidence for baroclinic energy conversion within the jet core at ~0.5 mb. By contrast, the fast waves exhibit relatively shallow baroclinic energy conversion.

[12] A striking aspect of the observed traveling wave behavior is the rapid disappearance of the slow wave 1 around solstice. This evidently reflects changes in the conditions required for the maintenance of this wave. In the MGCM simulation, the fast baroclinic wave and the *slow* wave are able to coexist relatively independently of each other during the $L_s = 230-270°$ interval and there is a hint of this behavior in the TES data as well. The slow wave structure appears to represent a coupling of an inertially-unstable circulation in low latitudes with a resonantly-enhanced, eastward propagating midlatitude Rossby wave. *Salby and Callaghan* [2001] described results suggesting that wave activity generated in unstable regions can disperse into normal mode structures. We envision a similar process in play here. The inertially-unstable region is maintained by the advection of easterly zonal wind into the NH by the Hadley circulation [*Barnes and Haberle*, 1996]. We speculate that the observed decline in dust opacity after $L_s = 235°$ led to a weakening of the thermal forcing which controls the intensity of the inertial instabilities. The Hadley circulation also influences the intensity of the baroclinic region defined by the circumpolar frontal zone. Further

work is underway to investigate the sensitivity of slowly propagating Rossby waves to variations in the configuration of the zonal mean temperature and zonal wind fields and to better understand the energy conversion processes that can maintain a large amplitude eddy structure.

References

Andrews, D. G., J. R. Holton, and C. B. Leovy, *Middle Atmosphere Dynamics*, 489 pp., Academic Press, Orlando, FL, 1987.

Banfield, D., B. J. Conrath, M. D. Smith, P. R. Christensen, and R. J. Wilson, Forced waves in the Martian atmosphere from MGS TES nadir data, *Icarus*, in press, 2002.

Banfield, D., J. R. Barnes, B. J. Conrath, J. C. Pearl, M. D. Smith, and P. Christensen, Atmospheric traveling waves from MGS TES, *Bull. Amer. Astron. Soc.*, 32, 1096 (abstract), 2000.

Banfield, D., B. J. Conrath, M. D. Smith, and R. J. Wilson, Mars transient and forced atmospheric waves from MGS TES: Climatology and inter-annual variability, *Bull. Amer. Astron. Soc.*, 33, 1067 (abstract), 2001.

Barnes, J. R., Time spectral analysis of midlatitude disturbances in the Martian atmosphere, *J. Atmos. Sci.*, 37, 2002–2015, 1980.

Barnes, J. R., Midlatitude disturbances in the Martian atmosphere: A second Mars year, *J. Atmos. Sci.*, 38, 225–234, 1981.

Barnes, J. R., Linear baroclinic instability in the martian atmosphere, *J. Atmos. Sci*, 41, 1536–1550, 1984.

Barnes, J. R., Asynoptic fourier transform analyses of MGS TES data: Transient baroclinic eddies, *Bull. Amer. Astron. Soc.*, 33, 1088 (abstract), 2001.

Barnes, J. R., et al., Mars atmospheric dynamics as simulated by the NASA Ames general circulation model, 2. Transient baroclinic eddies, *J. Geophys. Res.*, 98, 3125–3148, 1993.

Barnes, J. R., and R. M. Haberle, The martian zonal mean circulation: angular momentum and potential vorticity structure in GCM simulations, *J. Atmos. Sci.*, 53, 3143–4156, 1996.

Barnes, J. R., et al., Mars atmospheric dynamics as simulated by the NASA Ames general circulation model, 3. Winter quasi-stationary eddies, *J. Geophys. Res.*, 101, 12,753–12,776, 1996.

Collins, M., S. R. Lewis, P. L. Read, and F. Hourdin, Baroclinic wave transitions in the Martian atmosphere, *Icarus*, 120, 344–357, 1996.

Conrath, B. J., Planetary-scale wave structure in the Martian atmosphere, *Icarus*, 48, 246–255, 1981.

Conrath, B. J., et al., Mars Global Surveyor Thermal Emission Spectrometer observations: Atmospheric temperatures during aerobraking and science phasing, *J. Geophys. Res.*, 105, 9509–9519, 2000.

Hinson, D. P., and R. J. Wilson, Transient eddies in the southern hemisphere of Mars, *Geophys. Res. Lett.*, in press, 2002.

Hollingsworth, J. L., and J. R. Barnes, Forced stationary planetary waves in Mars's winter atmosphere, *J. Atmos. Sci.*, 53, 428–448, 1996.

Hollingsworth, J. L., R. M. Haberle, and J. Schaeffer, Seasonal variations of storm zones on Mars, *Adv. Space Res.*, 19, 1237–1240, 1997.

Salby, M. L., and P. F. Callaghan, Seasonal amplification of the 2-day wave: Relationship between normal mode and instability, *J. Atmos. Sci.*, 58, 1858–1869, 2001.

Wilson, R. J., Evidence for diurnal period Kelvin waves in the martian atmosphere from Mars Global Surveyor TES data, *Geophys. Res. Lett.*, 27, 3889–3892, 2000.

Wilson, R. J., and K. P. Hamilton, Comprehensive model simulation of thermal tides in the Martian atmosphere, *J. Atmos. Sci.*, 53, 1290–1326, 1996.

D. Banfield and B. J. Conrath, Department of Astronomy, Cornell University, Ithaca, NY 14853, USA. (banfield@astrosun.cornell.edu; barney@chryse.gsfc.nasa.gov)

M. D. Smith, NASA Goddard Space Flight Center, Greenbelt, MD 20771, USA. (Michael.D.Smith.1@gsfc.nasa.gov)

R. J. Wilson, NOAA/Geophysical Fluid Dynamics Laboratory, PO Box 308, Princeton, NJ 08542, USA. (rjw@gfdl.noaa.gov)